RSC Advances

ROYAL SOCIETY OF CHEMISTRY

www.rsc.org/advances

ARTICLE TYPE www.rsc.org/xxxxxx | XXXXXXXX

N-doped Carbon/MoS_2 Composites as an Excellent Battery Anode

Fan Yang,[a] Qiang Wan,[a] Xiaochuan Duan,[b,*] Wei Guo,[c,*] Yuhua Mao[d] and Jianmin Ma[a,*]

Received (in XXX, XXX) Xth XXXXXXXXX 200X, Accepted Xth XXXXXXXXX 200X
First published on the web Xth XXXXXXXXX 200X
DOI: 10.1039/b000000x

In this work, we have synthesized N-doped carbon/MoS_2 (C/MoS_2) composites by a simple hydrothermal method. It was found that the C/MoS_2 composite manifested high specific capacity of 611 mAh g^{-1} and excellent cycling performance than bare MoS_2 and N-doped carbon.

Lithium-ion batteries (LIBs) have become one of the main power sources for portable electronic devices and electric vehicles (EVs) due to its no memory effect, high energy densities, and good cycling stability.[1-3] At present, graphite is one of the most common anode materials, however, it has low theoretical specific capacity (372 mAh g^{-1}).[4] The further development of LIBs has been limited to the capacity of anode materials in a large scale. Thus, scientists turned to study the transition metal materials as potential anodes, such as metals, metal oxides, and metal sulfides.[5-12] In this case, layered molybdenum disulfide (MoS_2) has become one of the most promising alternatives. The reaction type of Li^+ inserted into molybdenum disulfide layered is: $MoS_2 + 4Li^+ + 4e^- = Mo + 2Li_2S$.[13, 14] So it has been regarded as a potential anode material in LIBs.[15] However, the reversibility of MoS_2 was found to be poor.[16] To date, some synthetic methods have been proposed to improve the cycling performance of MoS_2, such as integrating MoS_2 with different carbonaceous materials, like amorphous carbon,[17, 18] graphene[19-22] and carbon nanotubes (CNTs)[23-25] and so on. N-doped carbon derived from zeolitic imidazolate framework-8 (ZIF-8) exhibits porous structure, and has high specific surface area.[26]

In the communication, we have successfully synthesized the C/MoS_2 composites by a simple hydrothermal method using N-doped carbon polyhedron as the nucleus of MoS_2. The as-synthesized samples were characterized by a series of technologies, such as X-ray diffraction (XRD), scanning electron microscopy (SEM), transmission electron microscopy (TEM), Brunauer-Emmett-Teller (BET) analysis and X-ray photoelectron spectroscopy (XPS). The formation mechanism of C/MoS_2 composites was also proposed. When tested as anode material, the as-synthesized C/MoS_2 composites manifested high specific capacity and excellent cycling performance than bare MoS_2 and N-doped carbon.

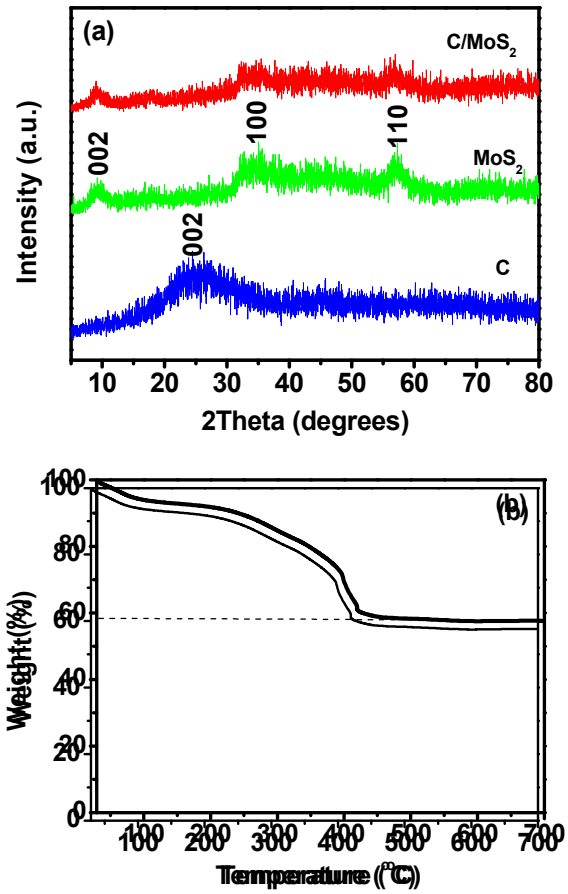

Fig. 1 (a) XRD patterns of C, MoS_2 and C/MoS_2; (b) TGA curve of C/MoS_2.

XRD characterization was performed to confirm structures of the as-synthesized three samples. As shown in Fig. 1a, all the diffraction peaks of MoS_2 and C/MoS_2 could be indexed to the rhombohedral structure of MoS_2. The thermal gravimetric analysis (TGA in Fig. 1b) was used to determine the amount of MoS_2 and N-doped carbon in the C/MoS_2 composite. In Fig. 1b, it can be seen that the weight loss totally was measured about 40%. Among these, nearly 10% of the mass loss occurred at about 100 °C, which is due to the existence of the adsorbed water in the sample. So the weight loss of the composite material due to react at is about 30%. To the reaction phase, the first weight loss at about 360 °C was attributed to the oxidation of MoS_2 to MoO_3. The second time weight loss occurs at about 420 °C caused by the combustion of the N-doped carbon. Through the fact that molybdenum

content remains constant, the content of N-doped carbon was calculated to be about 25% in the C/MoS_2 composite.

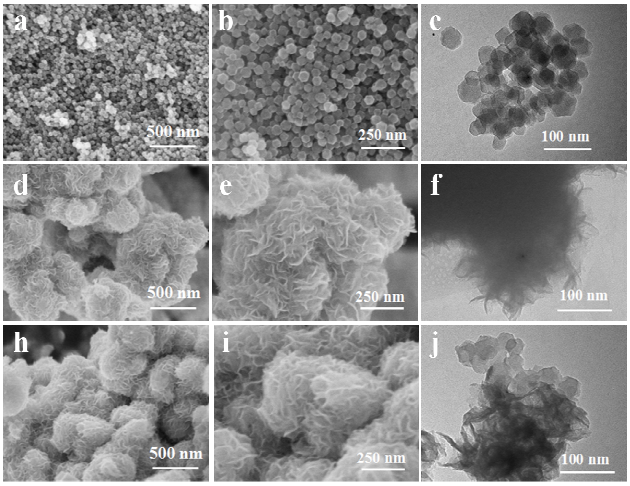

Fig. 2 (a, b and c) SEM and TEM images of C; (d, e and f) SEM and TEM images of MoS_2; (h, i and j) SEM and TEM images of C/MoS_2.

Fig. 2 shows the morphology of the as-synthesized of C, MoS_2 and C/MoS_2, respectively. In SEM image (Fig. 2a, b) and TEM image (Fig. 2c), we could find out that the C sample is composed of regular N-doped carbon polyhedron, which were prepared via removing ZnO by acid treatment, followed by annealing ZIF-8. The C sample has a size of about 50nm. As shown in SEM image (Fig. 2d, e) and TEM image (Fig. 2f), the MoS_2 sample is composed of nanoflowers assembled by nanosheets with a thickness of less than 10 nm. Fig. 2h, i and j present SEM and TEM images of C/MoS_2 sample, which has a similar morphology with MoS_2 nanoflowers. In addition, some N-doped carbon polyhedron can observed, as shown in Fig. 2j. Here, the formation of MoS_2 nanoflowers can be mainly attributed to its crystal growth habit.[10]

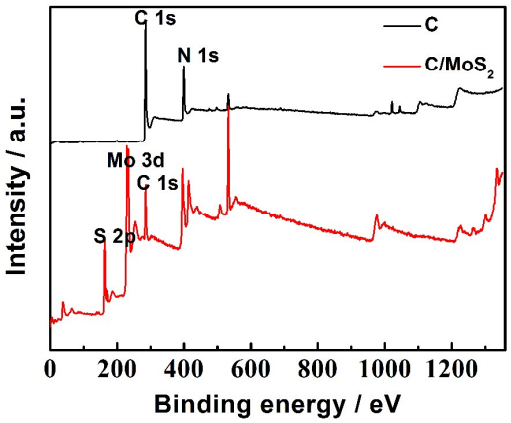

Fig. 3 The XPS survey spectrum of C/MoS_2 and C samples.

The elemental compositions of C/MoS_2 and C samples were analysed by (XPS). Fig. 3 presents the survey spectrum of C/MoS_2 and C samples, respectively. The content of N element is 5.84 % and 24.23 % for C/MoS_2 and C samples, respectively. Fig. S1a and 1b present the S_{2p} and Mo_{3d} spectrum of C/MoS_2, respectively. The S_{2p} spectrum in Fig. S1a was deconvoluted to two individual peaks, while the Mo_{3d} spectrum in Fig. S1b was deconvoluted to three individual peaks. Fig. S1c and d present the N_{1s} XPS spectrum of C/MoS_2 and C samples, respectively. In this work, nitrogen types can be divided into pyridinic N (398.7 eV), pyrrolic N (400.3 eV), graphitic N, 401.2 eV), and oxidized N (402.8 eV), respectively.[27] The content of pyridinic N, pyrrolic N, graphitic N and oxidized N in N-doped C polyhedron is 10.8 %, 6.7 %, 5.9%, 0.9 %, respectively, while the content of pyridinic N, pyrrolic N, graphitic N and oxidized N in C/MoS_2 is 0.9 %, 0.6 %, 0.6 %, 0.1 %, respectively. In addition, Fig. S2 shows the N_2 adsorption-desorption isotherm and corresponding pore size distributions of three samples. It also indicates that the specific surface area of C, MoS_2 and C/MoS_2 samples is 610, 13.6 and 23 $m^2 g^{-1}$, respectively. The data shows that the specific surface area of the composite is bigger than pure MoS_2. And this should be caused by the combination of C materials.

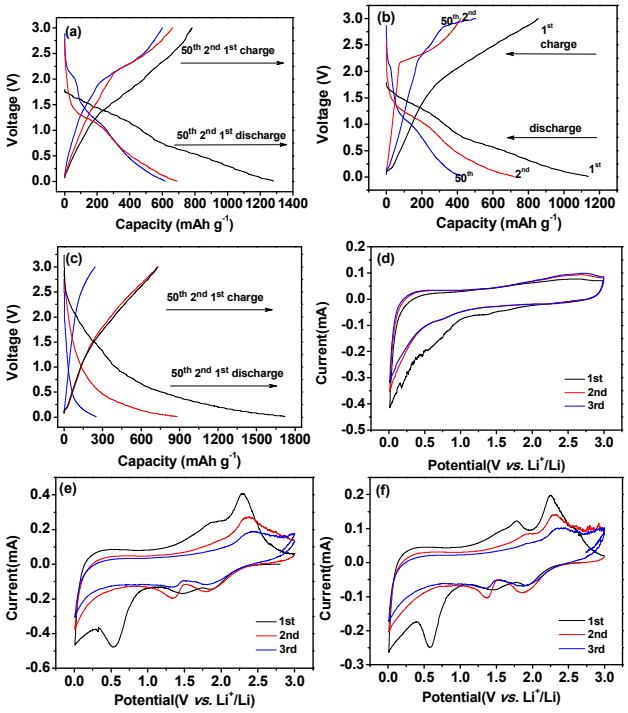

Fig. 4 (a-c) the charge-discharge curves of C/MoS_2, MoS_2 and C samples; (d-f) the cyclic voltammograms (CVs) for the first 3 cycles of C, MoS_2 and C/MoS_2 samples at a scan rate of 0.2 mV s^{-1}.

Fig. 4a-c shows the charge/discharge voltage profiles of the C, MoS_2 and C/MoS_2 electrodes at a current density of 50 mA g^{-1}. As shown in Fig. 4a-c, there is the large irreversible capacity loss, which is mainly because of the formation of the SEI film in the initial cycle. To investigate the electrochemical performance of the C, MoS_2 and C/MoS_2 samples as the LIB anodes, the cyclic voltammetry (CV) measurements were carried out in the potential window of 0.01-3.0V at a scan rate of 0.2 mV s^{-1}. Fig. 4d-f shows the CV curves for the first 3 cycles of C, MoS_2 and C/MoS_2 samples at a scan rate of 0.2 mV s^{-1}. In the first cathodic process in Fig. 4f, two reduction peaks at about 1.9V and 1.5V are showing Li intercalation into MoS_2 and conversion into Mo and Li_2S by the following two reactions:

$$MoS_2+xLi^++xe^-=Li_xMoS_2 \quad (1)$$

$$Li_xMoS_2+4Li^++4e^-=2Li_2S+Mo/Li_x \quad (2)$$

While the third reduction peak at about 0.55V could be due to the decomposition of the irreversible electrolyte. In the anodic scanning, two oxidation peaks appear at approximately 2.25V and 1.78V, represents the oxidation reaction from Mo to Mo^{4+} and Mo^{6+}, Li_2S to sulfur. In the later cycles, the reduction peaks at 1.82V and 1.33V are due to the reductions/oxidations between Mo and Mo^{6+}, and the oxidation peaks at 2.3V and 1.9V is the sulfide redox reaction.

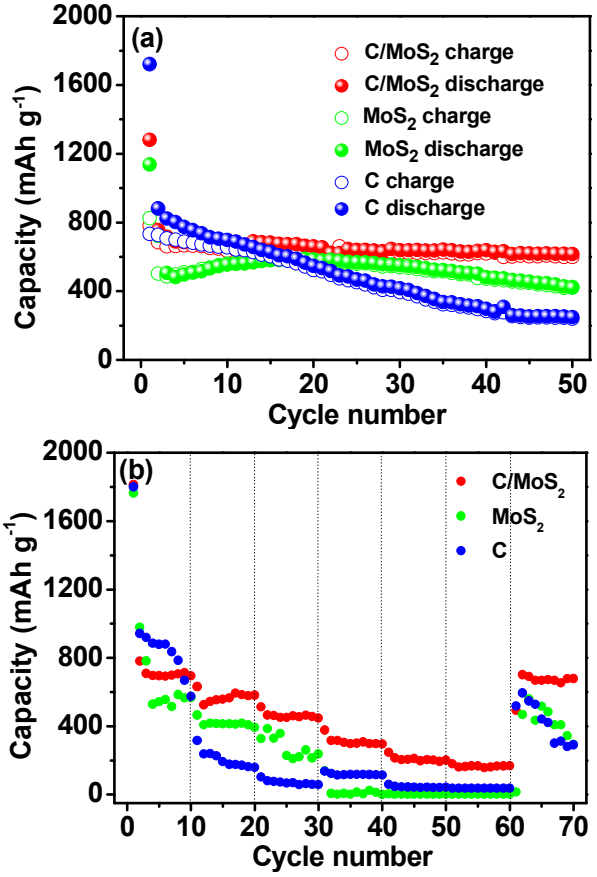

Fig. 5 (a) Cycling performance of the three samples; (b) Rate capability of three electrodes at various current densities between 0.01 and 3 V.

Fig. 5a shows the cycling performance of the C, MoS_2 and C/MoS_2 electrodes. Among the three electrodes, the C/MoS_2 electrode shows the highest storage capacity in comparison with the other electrode materials. The discharge/charge capacities in the 1st cycle are 1284/783 mAh g^{-1} for the C/MoS_2, while 1712/740 mAh g^{-1} for the C sample and 1143/514 mAh g^{-1} for the MoS_2 sample, respectively. After 50 cycles, the discharge/charge capacities of the C/MoS_2 electrode still remain at 611/605 mAh g^{-1}, respectively, indicating better electrochemical performance than the C and MoS_2 samples. In Fig. S3, the coulombic efficiencies of C, MoS_2 and C/MoS_2 electrodes are above 99%, except for the first cycle. Fig. 5b shows the discharge capabilities of the C, MoS_2 and C/MoS_2 electrodes at different current densities between 50 mA g^{-1} and 1000 mA g^{-1}, respectively. The C/MoS_2 electrode clearly shows a higher specific capacity than the other electrodes after 10 cycles. The discharge capacity drops gradually as the current density increases for the three samples. For the C/MoS_2 electrode, the discharge specific capacities are 708, 588, 458, 302, 201 and 165 mAh g^{-1} at 50, 100, 200, 500, 800 and 1000 mA g^{-1}, respectively. While the discharge capacity of the C and MoS_2 electrodes are only 886/546, 409/165, 237/70, 140/32, 46/15 and 33/15 mAh g^{-1} at the same rate. The reversible capacity restores to 684 mAh g^{-1} when the discharge rate returns back to 50 mA g^{-1}, which is higher than the C and MoS_2 electrodes. These results indicate that those of the C/MoS_2 electrode shows better cycling performance and rate performance than the C and MoS_2 electrodes. The enhanced electrochemical performance of the C/MoS_2 electrode can be attributed to the hybrid structure, which can improve the electric conductivity of electrode and keep high capacity. In Fig. S4 shows the Nyquist plots of the C, MoS_2 and C/MoS_2 electrodes at open potential before cycling test. In similar with the impedance spectra of other MoS_2-based electrodes, the impedance spectroscopy is composed of low frequency semicircle and high frequency of straight line. From the impedance curves of the materials, we know that the electrical conductivity of C/MoS_2 is better than pure MoS_2, which is used to explain the excellent performance of C/MoS_2.

In summary, we have fabricated the C/MoS_2 composites by solvothermal method. The as-synthesized C/MoS_2 shows significantly improved cycling performance with a high capacity of 611 mAh g^{-1} after 50 cycles at a current density of 50 mA g^{-1}, much better than the bare C and MoS_2 samples as anode materials for LIBs. This method might be extended to the synthesis of other composite materials to enhance the energy storage capacity and rate ability.

Acknowledgements

This work was supported by the National Natural Science Foundation of China (Grant No. 51302079).

Notes and references

[a]*Key Laboratory for Micro-/Nano-Optoelectronic Devices of the Ministry of Education, School of Physics and Electronics, Hunan University, Changsha 410082, P. R. China. Email: nanoelechem@hnu.edu.cn*

[b]*Pen-Tung Sah Institute of Micro-Nano Science and Technology, Xiamen University, Xiamen, P. R. China. xcduan@xmu.edu.cn*

[c]*College of Chemistry and Chemical Engineering, Anyang Normal University, Anyang 455000, China*

E-mail: *wgnk@mail.nankai.edu.cn*

[d]*Shenzhen Capchem Technology Co., LTD, Shenzhen 518118, P. R. China*

† Electronic Supplementary Information (ESI) available: [details of any supplementary information available should be included here]. See DOI: 10.1039/b000000x/

‡ Footnotes should appear here. These might include comments relevant to but not central to the matter under discussion, limited experimental and spectral data, and crystallographic data.

1 Y. M. Shi, Y. Wang, J. I. Wong, A. Y. S. Tan, C. L. Hsu, L. J. Li, Y. C. Lu, and H. Y. Yang, *Scientific Reports*, 2013, **3**, 2169-2177.

2 K. Chang and W. X. Chen, *ACS Nano*, 2011, **5**, 4720-4728.

3 W.D. Qiu, J. Xia, S. X. He, H. J. Xu, H. M. Zhong and L. P. Chen, *Electrochimica Acta.*, 2014, **117**, 145-152.

4 F. Y. Xiong, Z. Y. Cai, L. B. Qu, P. F. Zhang, Z. F. Yuan, O. K. Asare, W. W. Xu, C. Lin and L. Q. Mai, *ACS Appl. Mater. Interfaces*, 2015, **7**, 12625-12630

5 X. Li, W. Guo, Q. Wan and J. M. Ma, *RSC Adv.*, 2015, **5**, 28111-28114.

6 X. Zhou, Z. Dai, S. Liu, J. Bao, Y.-G. Guo, *Adv. Mater.*, 2014, **26**, 3943-3949.

7 L. Wang, B. Y. Ruan, J. T. Xu, H. K. Liu and J. M. Ma, *RSC Adv.*, 2015, **5**, 36104-36107.

8 G. Zhao, T. Wen, J. Zhang, J. Li, H. Dong, X.-K. Wang, Y. G. Guo and W. P. Hu, *J. Mater. Chem. A*, 2014, **2**, 944-948.

9 Z. Y. Cai, L. Xu, M. Y. Yan, C. H. Han, L. He, K. M. Hercule, C. J. Niu, Z. F. Yuan, W. W. Xu, L. B. Qu, K. N. Zhao, L. Q. Mai, *Nano Lett.*, 2015, **15**, 738-744.

10 C. Y. Cui, X. Li, Z. Hu, J. T. Xu, H. K. Liu and J. M. Ma, *RSC Adv.*, 2015, **5**, 92506-92514.

11 L. Chang, L. Q. Mai, X. Xu, Q. Y. An, Y. L. Zhao, D. D. Wang and X. Feng, *RSC Adv.*, 2013, **3**, 1947–1952.

12 H. S. Lee, S. W. Min, Y. G. Chang, M. K. Park, T. Nam, H. Kim, J. H. Kim, S. Ryu and S. Im, *Nano Lett.*, 2012, **12**, 3695-3700.

13 Y. C. Liu, Y. P. Zhao, L. F. Jiao and J. Chen, *J. Mater. Chem. A*, 2014, **2**, 13109-13115.

14 Q. F. Zhang, K. Yu, B. Zhao, Y. Wang, C. Q. Song, S. C. Li, H. H. Yin, Z. L. Zhang and Z. Q. Zhu, *RSC Adv.*, 2013, **3**, 10994-11000.

15 M. Wang, G. D. Li, H. Y. Xu, Y. T. Qian, and J. Yang, *ACS Appl. Mater. Interfaces*, 2013, **5**, 1003-1008.

16 L. Ma, W. X. Chen, L. M. Xu, X. P. Zhou and B. Jin, *Ceramics International*, 2012, **38**, 229-234.

17 Y. E. Miao, Y. P. Huang, L. S. Zhang, W. Fan, F. L. Lai and T. X. Liu, *Nanoscale*, 2015, **7**, 11093-11101.

18 J. W. Zhou, J. Qin, X. Zhang, C. S. Shi, E. Z. Liu, J. J. Li, N. Q. Zhao and C. N. He, *ACS Nano*, 2015, **4**, 3837-3848.

19 B. Radisavljevic, A. Radenovic, J. Brivio, V. Giacometti and A. Kis, *Nat. Nanotechnol*., 2011, **6**, 147-510.

20 K. Chang and W. X. Chen, *Chem. Commun.*, 2011, **47**, 4252-4254.

21 H. L. Li, K. Yu, H. Fu, B. J. Guo, X. Lei and Z. Q. Zhu, *J. Phys. Chem. C*, 2015, **119**, 7959-7968.

22 D. B. Kong, H. Y. He, Q. Song, B. Wang, W. Lv, Q. H. Yang and L. J. Zhi, *Energy Environ. Sci.*, 2014, **7**, 3320-3325.

23 X. Y. Yu, H. Hu, Y. W. Wang, H. Y. Chen and X. W. Lou, *Angew. Chem. Int. Ed.*, 2015, **54**, 7395-7398.

24 S. J. Ding, J. S. Chen and X. W. Lou, *Chem. Eur. J.*, 2011,**17**, 13142-13145.

25 R. J. Chen, T. Zhao, W. P. Wu, F. Wu, L. Li, J. Qian, R. Xu, H. M. Wu, H. M. Albishri, A. S. Al-Bogami, D. A. El-Hady, Jun Lu and K. Amine, *Nano Lett.*, 2014, **14**, 5899-5904.

26 L. J. Zhang, Z. X. Su, F. L. Jiang, L. L. Yang, J. J. Qian, Y. F. Zhou, W. M. Lia and M. C. Hong, *Nanoscale*, 2014, **6**, 6590-6602.

27 L. Wang, S. Dou, J. T. Xu, H. K. Liu, S. Y. Wang, J. M. Ma and S. X. Dou, *Chem. Commun.*, 2015, **51**, 11791-11794.

Graphical Abstract

N-doped Carbon/MoS_2 Composites as an Excellent Battery Anode

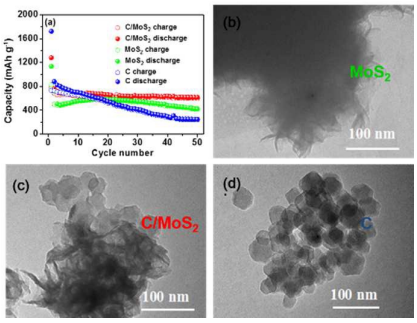

In this work, we have synthesized N-doped carbon/MoS_2 (C/MoS_2) composites by a simple hydrothermal method. It was found that the C/MoS_2 composite manifested high specific capacity of 611 mAh g^{-1} and excellent cycling performance than bare MoS_2 and N-doped carbon.